AAPS Open

RESEARCH

Open Access

Verification of nanoparticle formation, skin permeation, and apoptosis using nobiletin as a methoxyflavonoid derivative

Yutaka Inoue[1*], Moe Ishizawa[1], Shoko Itakura[2], Takashi Tanikawa[1] and Hiroaki Todo[2]

Abstract

Purpose: Nobiletin (NOB), a polymethoxyflavonoid, is known for its antioxidant and anti-inflammatory effects and has antitumor activity. However, its poor solubility and low bioavailability pose a significant challenge in its delivery. In this experiment, NOB was added to Soluplus® (Sol)/L-ascorbyl 2,6-dipalmitate (ASC-DP) as a ternary system, and Sol/ASC-DP/NOB nanoparticles were obtained using the hydration method. The purpose of this study was to enhance the solubility of NOB, apply it for skin permeation, and improve antitumor activity.

Methods: The preparation of Sol/ASC-DP/NOB nanoparticles was attempted using the hydration method, and particle size, zeta potential, and stability tests were performed to evaluate the formation of nanoparticles. 1H-1H NOESY/ROESY NMR spectral measurements were also performed to identify molecular interaction between NOB and Sol/ASC-DP. To evaluate its functionality, DPPH radical scavenging, skin permeation, fluorescence microscopy, and cell viability analyses were performed.

Results: The particles were approximately 100 nm in size in the ternary system (weight ratio (Sol/ASCDP/NOB=8/1/1)) and were relatively stable for approximately 7 days at 25 °C under light-shielded conditions. From the NMR spectrum measurements of Sol/ASCDP/NOB, a cross-peak was observed between the –OCH3 group: C6,8 (3.8 ppm) derived from NOB, the methyl group (2.0 ppm) derived from Sol, and the side chain portion (1.2 ppm) derived from ASC-DP. Cross-peaks were observed between the polyethylene glycol (PEG) backbone of Sol (3.6 ppm) and the side chain of ASC-DP (0.8–1.2 ppm). The formation of Sol/ASC-DP/NOB nanoparticles facilitated its skin permeation, and fluorescence microscopy confirmed improved permeation. The DPPH radical scavenging test revealed that Sol/ASC-DP/NOB had an IC_{50} of 46.7 μg/mL. Cell viability assays showed a 20–40% decrease in cell viability with the addition of Sol/ASC-DP/NOB at 0.1 mg/mL.

Conclusion: Sol/ASC-DP/NOB nanoparticles were successfully prepared, and these were found to inhibit melanin formation and have antitumor activity.

Keywords: Nobiletin, Nanoparticle, Cell viability, Skin permeation, NMR spectrum

Introduction

Nobiletin (NOB) is a polymethoxyflavonoid found in citrus fruits (Hattori et al., 2019). It has a variety of physiological effects, including anti-Alzheimer's disease (Matsuzaki et al., 2006; Seki et al., 2013), anti-inflammatory (Lin et al., 2003a), anti-cancer effects by inhibiting angiogenesis (Kunimasa et al., 2010), improvement of memory impairment (Nagase et al., 2005), and

*Correspondence: yinoue@josai.ac.jp

[1] Laboratory of Nutri-Pharmacotherapeutics Management, Faculty of Pharmacy and Pharmaceutical Sciences, Josai University, 1-1 Keyakidai, Sakado, Saitama 3500295, Japan
Full list of author information is available at the end of the article

anti-diabetes (Hattori et al., 2019). However, NOB has an extremely low solubility of 16.2 μg/mL (Onoue et al., 2011). The oral absorption of NOB can be improved by preparing solid dispersions (Onoue et al., 2011; Onoue et al., 2013), self-emulsifying emulsions (Yao et al., 2008), nanoparticles (Luque-Alcaraz et al., 2012), self-assembled prolisosomes (Lin et al., 2009), and improved transdermal delivery using ionic liquids (Hattori et al., 2019). However, because of the highly lipophilic nature of the flavonoid structure, the oral bioavailability of NOB is also very low (0.85%), and a sufficient remedy has not yet been achieved (Onoue et al., 2011). Nobiletin has also attracted attention as an ingredient with skin nutraceutical properties such as antioxidant (Murakami et al., 2000) and anti-inflammatory effects (Lin et al., 2003b; Lai et al., 2008). Therefore, we focused on the skin chemopreventive properties of NOB in this study as well. Therefore, a breakthrough in NOB formulation is required to expand its utilization.

In recent years, various drug delivery systems (DDS) have been developed for different routes of administration, such as emulsions, liposomes, solid lipid nanoparticles, micelles, and *polymeric* nanoparticles. These are used to improve physical properties and pharmacokinetics. In particular, variations may improve pharmacological effects, reduce side effects, and reduce the frequency of administration by improving absorption, prolonging half-life by controlled release, and targeting specific tissues. These drug systems have been developed in various fields, such as cosmetics, food chemistry, and pharmaceuticals (Onoue et al., 2014; Sun et al., 2014). It is also feasible to modify the application by modifying the surface properties by changing the composition, morphology, surface charge, functional groups, and PEGylation of nanocarriers to improve their physicochemical properties (Zhang et al., 2014).

Soluplus® (Sol; polyvinyl caprolactam-polyvinyl acetate-polyethylene glycol graft copolymer) has a polyethylene glycol (PEG) structure, as the hydrophilic part, with an amphiphilic copolymer with vinyl caprolactam/vinyl acetate side chains. It is known to improve the solubility of poorly water-soluble substances by forming self-assembled micelles (Zeng et al., 2017). In addition, Sol acts as a stabilizer, enabling the formation of fine stable particles (Yang et al., 2014). Sol has been confirmed to have a low critical micelle concentration of 0.82 mg/mL, and because of its properties, it exhibits high dispersibility upon dilution (Dian et al., 2014). Additionally, we succeeded in preparing novel nanoparticles using L-ascorbyl 2,6-dipalmitate (ASC-DP), and Sol, an amphiphilic copolymer, and further improved drug delivery into the skin by encapsulating minoxidil in the prepared nanoparticles (Takayama et al., 2021).

ASC-DP is an ascorbic acid derivative synthesized to improve the stability of ascorbic acid (ASC) (Palma et al., 2007). ASC is a water-soluble vitamin C with antioxidant properties and is widely used as an additive in foods and pharmaceuticals (Meister, 1994). It has a whitening effect by reducing pigmentation and decomposing melanin and a wrinkle-reducing effect by stimulating collagen synthesis and improving skin elasticity (Kameyama et al., 1996). However, it is susceptible to degradation by heat and light and has low stability (Palma et al., 2007). ASC-DP does not spontaneously aggregate when combined with surfactants to form nanoparticles (Moribe et al., 2010a). It is used in sunscreens and skin care products and is also being investigated in the development of cosmetics that provide whitening effects.

The successful formation of Sol/ASC-DP/NOB nanoparticles using an innovative and sustainable preparation method would improve the effect of NOB solubilization, the anti-cancer activity of NOB, and the synergistic effects of ASC-DP, such as antioxidant activity and dermal adaptation. Therefore, we attempted to prepare Sol/ASC-DP/NOB nanoparticles using the hydration method and performed particle size, zeta potential, and stability tests to evaluate the particulate formation. We also verified the physicochemical properties through ^{1}H-^{1}H NOESY/ROESY NMR spectroscopy, differential scanning calorimetry (DSC), and Fourier transform infrared spectrometer (FT-IR) measurements, and the functional properties through DPPH radical scavenging test, skin permeability test, fluorescence microscopy, and cell viability measurement.

Materials and methods

Materials

The Sol used was provided by BASF Japan Ltd. (lot: 84414368E0). ASC-DP was purchased from Tokyo Chemical Industry Co., Ltd. (Lot: ISPKK-LH). NOB was purchased from Toronto Research Chemicals (lot: 53-GHZ-8-1) (Fig. 1). NMR solvent ($CDCl_3$, 99.96%) was purchased from Cambridge Isotope Laboratories, Inc. (MA, USA). Saline and 5% glucose solutions were purchased from Otsuka Pharmaceutical Co. (Tokyo, Japan). Other reagents were purchased from commercial special-grade products (FUJIFILM Wako Pure Chemical Corporation, Tokyo, Japan). A375 cells were purchased from the European Collection of Authenticated Cell Cultures (Salisbury, UK), B16 and 4T1 cells were purchased from the JCRB Cell Bank (Osaka, Japan), and HaCaT cells were purchased from the Cell Line Service (Eppelheim, Germany). DPPH was purchased from Sigma–Aldrich (St. Louis, MO, USA).

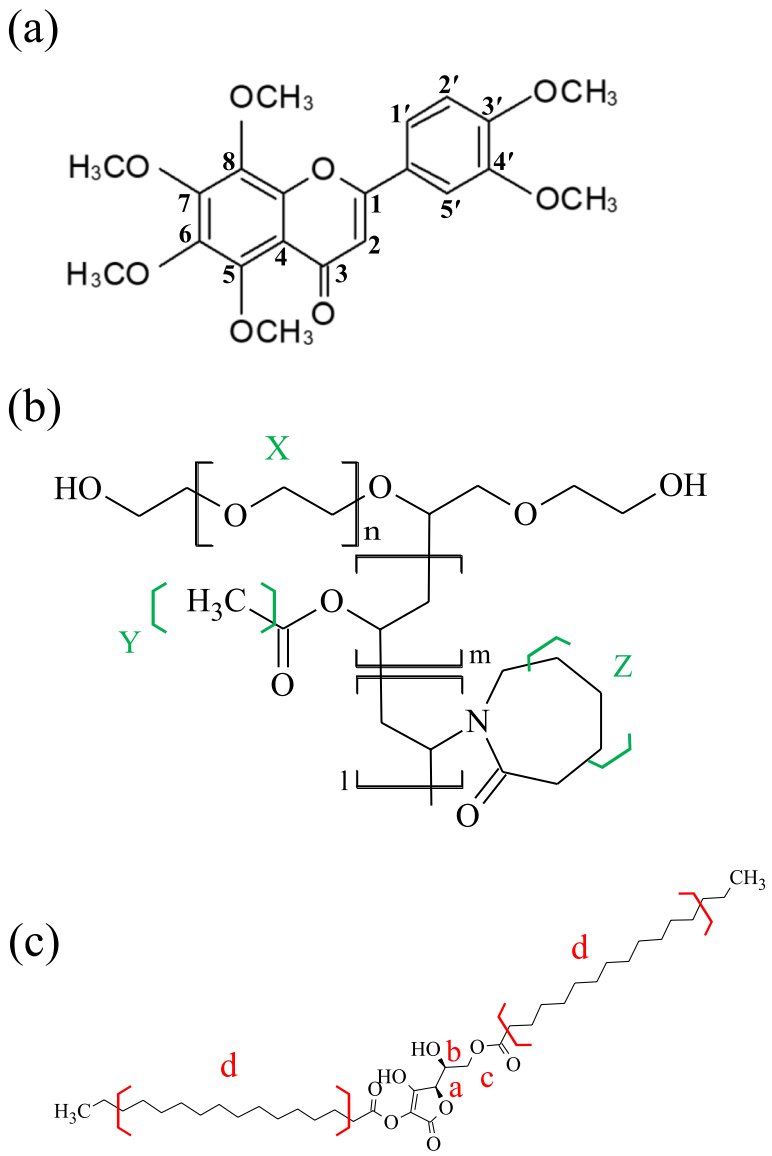

Fig. 1 Chemical structure. **a** Nobiletin (NOB), **b** Soluplus® (Sol), and **c** L-ascorbyl 2, 6-dipalmitate (ASC-DP)

Methods

Solvent-evaporated nanoparticles

The microparticles were prepared using the hydration method. The hydration method involves the preparation of a suspension or a solution by dissolving each lipid-soluble substance in an organic solvent, removing the solvent using an evaporator, and hydrating the prepared lipid film in an aqueous solvent, such as distilled water or saline. Sol, ASC-DP, and NOB were prepared at a 1-mg/mL concentration using 1 mL of chloroform, and Sol/ASC-DP/NOB was mixed and sonicated in a pear-shaped flask at a weight ratio of 8/1/1. The critical micelle concentration of Sol was 0.82 mg/mL (Tanida et al., 2016). These samples were evaporated (Rotavapor R-215, Buchi, Switzerland) at 40 °C to prepare the solvent-evaporated nanoparticles (EVP). The thin films were then hydrated with purified water to prepare nanoparticles.

Physical mixture (PM)

The PM was prepared by weighing Sol/ASC-DP/NOB at a weight ratio (8/1/1) and mixing with a vortex mixer for 1 min.

Measurement methods

Particle size measurement and zeta potential measurement

Particles dispersed in water were analyzed using a Zetasizer Nano ZS (Malvern Instruments, Malvern, UK) to measure mean particle size and polydispersity

index (PDI). In addition, the zeta potential was measured to evaluate the surface charge, which is thought to contribute to the stabilization of nanoparticles (Sol/ASC-DP/NOB = 8/1/1). One milliliter of each sample was added to the capillary cell, and measurements were performed under the following conditions: Set Zero 60 s (particle size), 120 s (zeta potential), and a measurement time of 180 s.

Stability test

To evaluate the stability of the prepared nanoparticles (Sol/ASC-DP/NOB = 8/1/1), they were stored in a dark room at 25 °C for 7 days. Particle size, PDI, and zeta potential measurements were performed at 0, 1, 3, 5, and 7 days, as described above. Nanoparticles in purified water, saline, and hydrated 5% glucose solutions were also prepared for the stability test as these solvents are commonly used diluents in clinical practice.

^{1}H-^{1}H NOESY/ROESY NMR spectrum measurement

Two-dimensional NMR measurements were performed using a Varian NMR System 700 MHz (Agilent Technologies, Santa Clara, CA, USA) to confirm the changes in molecular interactions in the solution of the EVP (Sol/NOB = 8/2) and EVP (Sol/ASC-DP/NOB = 8/1/1) in $CDCl_3$. Spectroscopic characteristics of the nanoparticles were measured using an NMR spectrometer (Varian System 700NB, Agilent) with an HCN probe operating at 699.7 MHz and a $CDCl_3$ solution. Other conditions were mixing time of 1500 ms (NOESY), 250 ms (ROESY), waiting for time 1 s, $CDCl_3$ as the solvent, and 256 integrated times at 25 °C.

Differential scanning calorimetry (DSC) measurement

DSC measurements were conducted using a high-sensitivity differential scanning calorimeter (Thermo plus Evo, Rigaku, Tokyo, Japan) to check the changes in the thermal behavior in the solid state of Sol/ASC-DP/NOB systems. Approximately 2 mg of each sample was placed in a sealed aluminum pan, and the measurement was performed at a heating rate of 5 °C/min in a nitrogen gas 60 mL/min airflow.

Infrared (IR) spectrometry

IR measurements were performed using a JASCO FT-IR 4600 (JASCO Corporation, Tokyo, Japan) to confirm the change in the interaction between molecules in the solid state of Sol/ASC-DP/NOB systems. This was achieved using the potassium bromide (KBr) plate method. The plate was prepared by sandwiching the sample between KBr plates, compressing, and forming with a press. Background correction was performed by using a blank plate. The measurement range was 4000–400 cm^{-1}.

DPPH radical scavenging test

To confirm the antioxidant power of Sol/ASC-DP/NOB=8/1/1 systems, a DPPH radical scavenging test was performed using a SPECTRA MAX microplate reader (Spectra Max 190, Molecular Devices Japan Co., Ltd., Tokyo, Japan). A DPPH stock solution was dissolved in ethanol to a final concentration of 40 μmol/L. Each test sample concentration dissolved in ethanol, 0.1 mol/L Tris buffer solution, and DPPH ethanol stock solution was added to a microplate to obtain a volume ratio of 2/2/1. Using a microplate reader, the mixture was incubated in the dark at 37 °C for 2 h, and the absorbance (As) of DPPH was measured at a wavelength of 517 nm. The inhibition rate was calculated from the obtained absorbance, and the inhibition concentration was 50%. The radical removal rate of a mixed solution (2/2/1) of ethanol/0.1 mol/L Tris solution/DPPH ethanol solution was 0% (A_0). A mixed solution of ethanol/0.1 mol/L Tris solution (3/2) was used as a radical removal rate of 100% (Bl: blank). The DPPH radical removal rate was calculated using the following formula:

$$\text{Radical scavenging activity} = \left[1 - (\text{As} - \text{Bl})/\left(\text{A}^0 - \text{Bl}\right)\right] \times 100$$

Skin permeability test

To evaluate the skin permeability of intact NOB and EVP (Sol/ASC-DP/NOB = 8/1/1), the amount charged was unified, and a skin permeability test was conducted for a comparative study with the NOB suspension and NOB-containing nanoparticle preparation (Sol/ASC-DP/NOB=8/1/1). As a pretreatment, YUCATAN micropig (YMPs, 5 months old, female, pig number: 72–020) skin, frozen and stored at −80 °C, was thawed at 4 °C before use. After thawing, subcutaneous fat was removed, and the skin was cut to approximately 2.5 × 2.5 cm. The stratum corneum (SC) was removed via tape stripping 30 times. The SC was removed to allow the estimation of permeation parameters such as K_{ved} and D_{ved} and aid in the prediction of NOB concentration in the skin. The treated YMP skin was approximately 2–3 mm thick. After removing the stratum corneum, the YMP skin was placed on a paper towel moistened with saline with the epidermis side up and stored at 4 °C for 20 h before use. The test used a Franz-type diffusion cell (Perme Gear, PA, USA, effective permeation area: approximately 0.95 cm^2) which was used for the permeability test following the method described by (Yamaguchi et al., 2008; Arce et al., 2020). The receiver compartment was filled with approximately 9.5 mL phosphate-buffered saline (pH 7.4; Thermo Fisher

Scientific Life Technology Japan Co., Ltd., Tokyo, Japan). During the permeation tests, the receiver compartment was maintained at 32 ± 2 °C and stirred. The YMP skin was placed on a Franz-type diffusion cell, with the epidermis as the donor side and the dermis side as the receiver compartment. Two milliliters of each NOB suspension and the prepared nanoparticles (Sol/ASC-DP/NOB = 8/1/1) were added dropwise to the donor side.

After 24 h of the permeation test, the YMP skin was removed from the Franz-type diffusion cell, the epidermal side was washed with saline, and the effective area was finely chopped. The finely chopped YMP skin (0.2 g) was added with 2 mL of acetonitrile and was homogenized (26000 rpm, 2 min) using POLYTRON® BIOTRONA® PT 2500 E. The homogenized material was centrifuged (4 °C, 2900 × *g*, 30 min) using a High-speed Microcentrifuge CF16RN (Yamato Corporation, Tokyo, Japan). After centrifugation, the supernatant was further centrifuged (4 °C, 21500 × *g*, 10 min) and filtered through a 0.45-μm membrane filter (ADVANTEC®, Toyo Roshi Company, Ltd., Tokyo, Japan) and was used during HPLC analysis. Determination of NOB in YMP skin was conducted using a Waters e2695 UV-Visible photometer (Waters Japan Ltd., Tokyo, Japan) under the following conditions: wavelength 336 nm; column Inertsil® ODS-3 column (ϕ 5 μm, 4.6 × 150 nm, GL Sciences Inc. Tokyo, Japan); column temperature, 40 °C; mobile phase, 1% aqueous phosphoric acid solution/acetonitrile = 1/1; injection volume, 50 μL; NOB retention time, adjusted to approximately 7 min. The detection limit was 1.5 ng/mL, and the quantification limit was 4.6 ng/mL.

Fluorescence microscope observation

Skin sections were evaluated by fluorescence microscopy to visualize the degree of permeation of NOB in the skin. The sample utilized was the effective area (i.e., formulation-applied region) of the YMP skin after 24 h of the skin permeability tests. A sample of the YMP skin (approximately 7.0 × 2.0 mm) was placed in a plastic-embedded dish and filled with Tissue-Tek® optimum cutting temperature (O.C.T.) Compound (Sakura® Finetek Japan K.K., Tokyo, Japan). The samples were completely frozen at −80°C. Sections made of the frozen skin samples were cut at a 0.2-μm thickness using LEICA CM3050S (Leica Biosystems, Nussloch, Germany) to prepare frozen sections. The prepared frozen sections were observed under an all-in-one fluorescence microscope BZ-X800 (manufactured by KEYENCE, Osaka, Japan). The sections were observed at an excitation wavelength of 340–390 nm.

Measurement of cell viability

A375 (human melanoma), B16 (mouse melanoma), 4T1 (mouse mammary tumor cell line), and HaCaT (human keratinocytes) cells were seeded in a 96-well plate at 3 × 10^3 cells/well at 37 °C and 5% CO_2 and incubated overnight. Purified water was added as solvent control. Sol alone, Sol/ASC-DP = 8/2, Sol/ASC-DP/NOB = 8/1/1, and So/NOB = 8/2 were added at total lipid concentrations of 0.1, 0.2, and 0.4 mg, respectively, and incubated for 24 h at 37 °C in 5% CO_2 conditions. Living cells were evaluated using a Cell Counting kit-8 (DOJINDO, Kumamoto, Japan) according to the manufacturer's instructions. Briefly, a Cell Counting kit solution was added at 10 μL/well, and the absorbance at 450 nm was measured using a microplate reader (Molecular Devices, CA, USA). The cell viability was calculated using the following formula:

$$\text{Cell viability (\%)} = [(\text{As} - \text{Ab})/(\text{Ac} - \text{Ab})] \times 100$$

As: Absorbance of the sample
Ac: Control (untreated) absorbance
Ab: Absorbance of blank (medium only)

Statistical analysis

Statistical analysis of the skin penetration tests was performed using Tukey's test. ** $p < 0.01$ and * $p < 0.05$ were considered significant differences. Statistical analysis of cell viability was performed using Dunnett's test and compared with those treated with distilled water, with significant differences at *** $p < 0.001$, ** $p < 0.01$, and * $p < 0.05$.

Results and discussion

Evaluation of Sol/ASC-DP/NOB particles

Particle size and zeta potential measurement

Nanoparticles are known to form in Sol and ASC-DP (Takayama et al., 2021). Consequently, the particle size and zeta potential measurements were performed to assess the particulate formulation of Sol/ASC-DP with NOB (Table 1). The average particle size of intact Sol was approximately 76.7 nm, and the zeta potential was demonstrated at approximately −4.4 mV. Because ASC-DP and NOB are insoluble in water, it was confirmed that intact ASC-DP was polydispersed between particle diameters of 100 and 5000 nm, and intact NOB was dispersed between particle diameters of 1000 and 2500 nm.

Mixed weight ratios (Sol/ASC-DP = 8/2, Sol/NOB = 8/2, ASC-DP/NOB = 1/1, and Sol/ASC-DP/NOB = 8/1/1, 8/1/ 2, 8/1/3, 9/1/1, and 9/1/2) were prepared and evaluated based on the particle size distribution and zeta potential. In the binary system Sol/ASC-DP = 8/2, it was confirmed that the average particle size was approximately 134.5 nm, and the zeta potential was approximately −25.9 mV. Precipitation could not be visually confirmed with Sol/NOB = 8/2, but the particle size appeared as polydisperse between 70 and 5600

Table 1 Particle size and zeta potential (ZP) of Sol/ASC-DP/NOB systems

Sample	Particle size (nm)	ZP (mV)
Soluplus	76.7 ± 0.4	−4.4 ± 0.3
ASC-DP	100~5000	−7.3 ± 3.3
NOB	1000~2500	−16.2 ± 0.4
Soluplus/ASC-DP = 8/2	134.5 ± 0.9	−25.9 ± 1.9
Soluplus/NOB = 8/2	70~5600	−3.9 ± 1.0
ASC-DP/NOB = 1/1	150~6000	−16.4 ± 0.4
Soluplus/ASC-DP/NOB = 8/1/1	92.8 ± 0.1	−15.5 ± 0.3
Soluplus/ASC-DP/NOB = 8/1/2	90~5000	−22.2 ± 0.6
Soluplus/ASC-DP/NOB = 8/1/3	80~5500	−16.1 ± 0.7
Soluplus/ASC-DP/NOB = 9/1/1	100~4700	−19.6 ± 3.2
Soluplus/ASC-DP/NOB = 9/1/2	100~4000	−16.8 ± 0.4

Results are expressed as mean ± S.D. (*n*=3)

nm. ASC-DP/NOB = 1/1 exhibited drug precipitation and a particle size between 150 and 6000 nm, which appeared polydisperse. The formation of nanoparticles in the binary system (Sol/ASC-DP = 8/2) was similar to that reported by Takayama et al. (Takayama et al., 2021). For the ternary system (Sol/ASC-DP/NOB = 8/1/1), an average particle size of approximately 92.8 nm and zeta potential of approximately −15.5 mV were observed (Fig. 2). Sol/ASC-DP/NOB was confirmed as multidispersive in a wide range of 90–5000 nm at 8/1/2, 80–5500 nm at 8/1/3, 100–4700 nm at 9/1/1, and 100–4000 nm at 9/1/2. This suggested that nanoparticles were formed at a mixed weight ratio (Sol/ASC-DP/NOB = 8/1/1).

The surface charge of the particles is essential in assessing their dispersibility and stability, and particles with a zeta potential of ± 30 mV or more are reported stable in suspension, as the surface charge prevents particle aggregation (Singh & Lillard, 2009). However, it has also been reported that sufficient stabilization is possible in the case of a high-molecular-weight stabilizer, even with a zeta potential of ± 20 mV or less (Mishra et al., 2009). It has been reported that Sol has a high molecular weight and is used as a stabilizer (Yang et al., 2014). Therefore, it is inferred that the zeta potential of the nanoparticles prepared with Sol/ASC-DP/NOB = 8/1/1 is relatively stable even at approximately −15.5 mV. Based on this result, a stability test was performed to evaluate the state of the nanoparticles after preparation and the validity of the zeta potential.

Stability test

To examine the stability of the prepared nanoparticles, a suspension was obtained using purified water, a 5% glucose solution, and saline as a dispersion medium prepared with EVP (Sol/ASC-DP/NOB = 8/1/1). These dispersion media are commonly used as pharmaceutical formulations for injections in clinical practice. These were evaluated for their 7-day stability under light-shielding conditions at 25 °C (Fig. 3).

On the first day of preparation (Fig. 3a), the saline solution was observed to have a particle size in the wide range of 100–1000 nm, and the zeta potential was −1.8 ± 0.1 mV. On the 7th day (Fig. 3b), the zeta potential was −2.3 ± 0.4 mV, which was observed polydispersed over a wide range of 50–6000 nm. Based on the above points, it is presumed that salting out occurred when physiological saline was added, which made the particles unstable.

The Sol/ASC-DP/NOB = 8/1/1particles suspended in 5% dextrose solution was measured to have particles approximately 109.1 ± 2.6 nm in size and −8.0 ± 0.4 mV in zeta potential on the first day (Fig. 3c). A large increase in particle size was observed on the 3rd day and on the 7th day (Fig. 3d), the particle size was observed at approximately 144.5 ± 15.9 nm, and the zeta potential was −21.2 ± 0.6 mV. On the 7th day, in addition to the particle size of 144.5 nm, a peak considered agglutination was widely observed in the range of 1000–4000 nm. The particles suspended in purified water were observed to

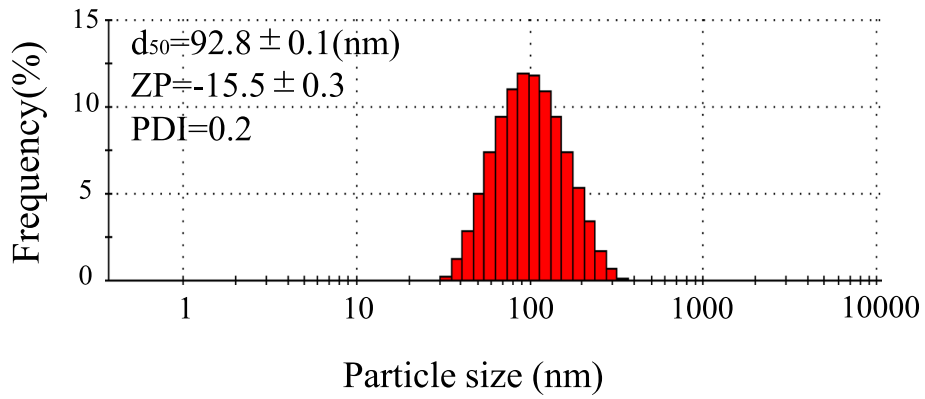

Fig. 2 Particle size and zeta potential of nanoparticles of Sol/ASC-DP/NOB = 8/1/1

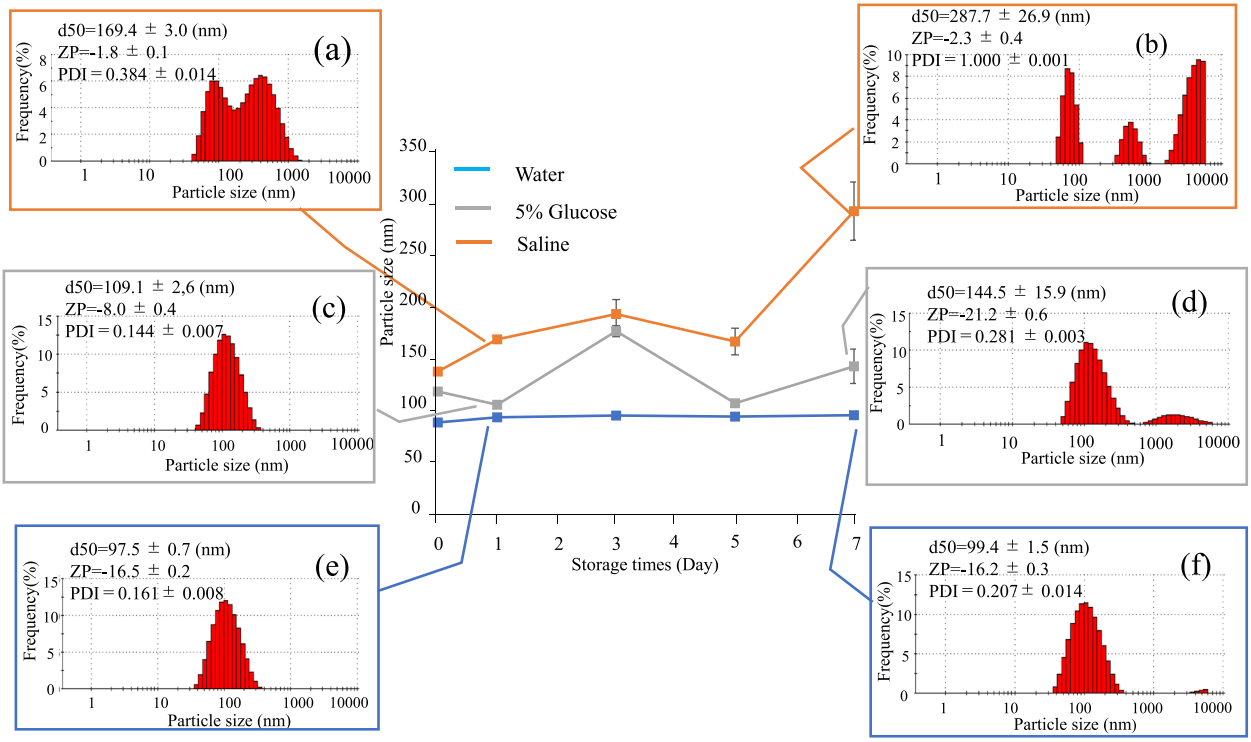

Fig. 3 Changes in particle size and zeta potential of nanoparticles of Sol/ASC-DP/NOB = 8/1/1 nanoparticles after the storage at 25 °C day 1 to day 7 in distilled water (DW), 5% glucose solution, and saline. Each point represents the mean ± S.D. **a** Day 1: saline, **b** day 7: saline, **c** day 1: 5% glucose, **d** day 7: 5% glucose, **e** day 1: DW, and **f** day 7: DW

be approximately 97.5 ± 0.7 nm and have a zeta potential of −16.5 ± 0.2 on the first day of preparation (Fig. 3e) and remained stable on the 7th day (Fig. 3f). In addition, the peak considered agglutination, seen at approximately 4000 nm on the 7th day, is extremely small, and most of them exist with a particle size almost the same as that on the 1st day, so it is inferred that the state is stable. The charge on the surface of the particles is essential in assessing the dispersibility and stability of the particles. However, it has also been reported that sufficient stabilization is possible in the case of a high-molecular-weight stabilizer, even with a zeta potential of ± 20 mV or less (Mishra et al., 2009). Those prepared with purified water showed no significant change in particle size, and the zeta potential remained unchanged from −16.5 to −16.2 mV from day 1 to day 7. Because Sol is a stabilizer of high molecular weight, the zeta potential of EVP (Sol/ASC-DP/NOB = 8/1/1) is ± 20 mV or less, which is a reasonable value that is inferred stable for 7 days. However, the 5% glucose solution showed a lower zeta potential (−8.0 mV on the first day of preparation), indicating an increase in particle size. Salting out was presumed to have occurred when saline was used as a dispersant, suggesting that EVP (Sol/ASC-DP/NOB=8/1/1) hydrated in purified water provided more stable nanoparticles.

^{1}H-^{1}H NOESY ROESY NMR spectral measurement

At Sol/ASC-DP/NOB=8/1/1, stable particle formation was observed. This suggests that the particle formation may be due to intermolecular interactions in the solution. Therefore, ^{1}H-^{1}H NOESY ROESY NMR measurements were performed to investigate intermolecular interactions in the solution (Fig. 4). The attribution of Sol is based on that reported by Xia et al. (Dengning et al., 2016). Molecular interactions in the binary component system (Sol/ASC-DP) were initially assessed. In EVP (Sol/ASC-DP=8/2) (Fig. 4), cross-peaks were observed between methyl groups Y (1.8–2.0 ppm) and 7-membered ring moiety Z (1.5–1.8 ppm) derived from Sol and CH groups a (4.8 ppm), b, and c (4.6–4.7 ppm) derived from ASC-DP (Fig. 4b).

No particle formation was observed for EVP (Sol/NOB = 8/2) and EVP (ASC-DP/NOB = 1/1), unlike Sol/ASC-DP/NOB = 8/1/1, suggesting that no intermolecular interaction occurred or that there were some differences. Measurements were also performed for EVP (Sol/NOB =

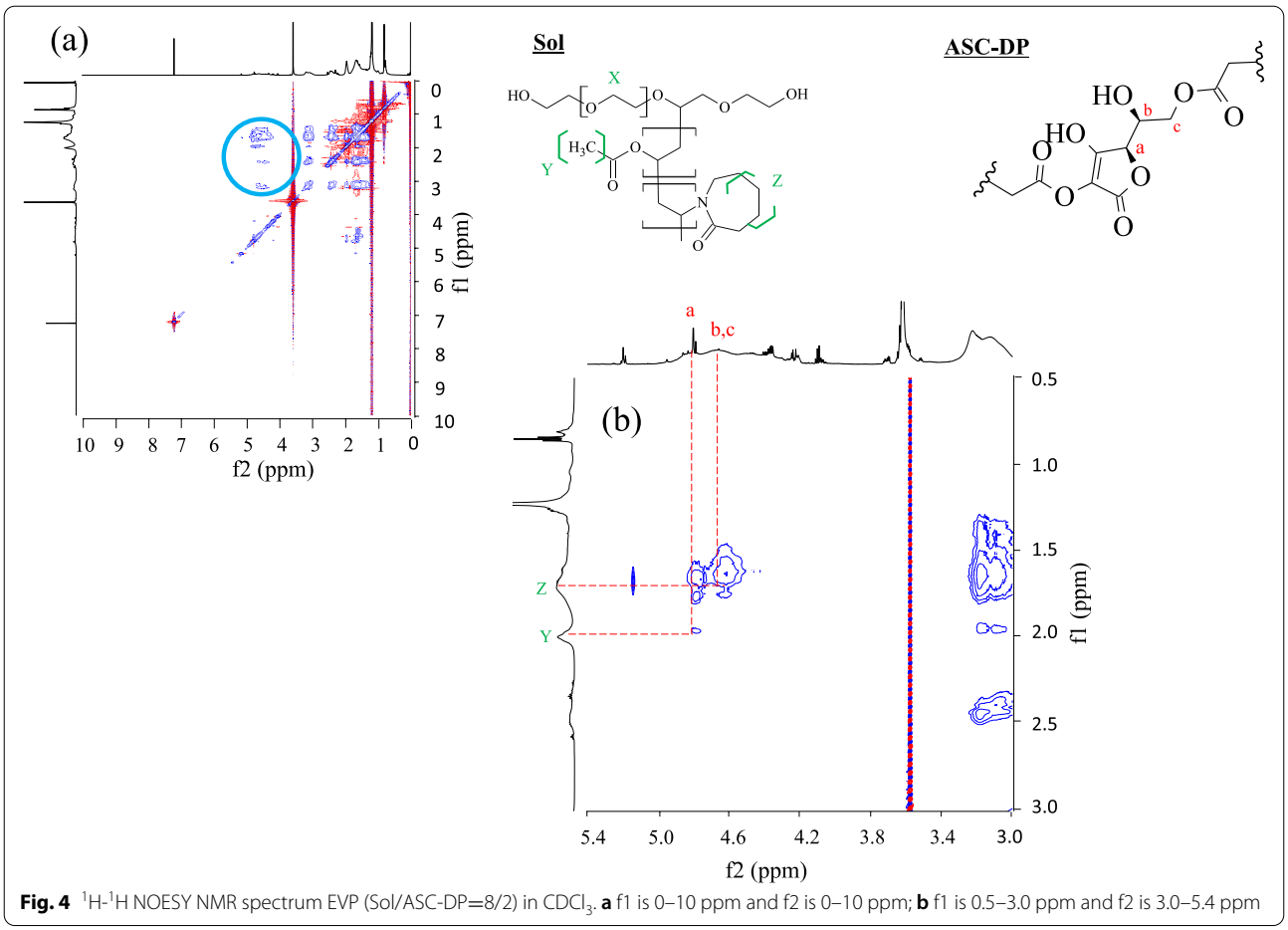

Fig. 4 ^{1}H-^{1}H NOESY NMR spectrum EVP (Sol/ASC-DP=8/2) in $CDCl_3$. **a** f1 is 0–10 ppm and f2 is 0–10 ppm; **b** f1 is 0.5–3.0 ppm and f2 is 3.0–5.4 ppm

8/2) and EVP (ASC-DP/NOB = 1/1). In EVP (Sol/NOB = 8/2) (Fig. 5), a cross-peak was identified between the PEG structure moiety: X (3.6 ppm) of Sol and the aromatic moieties 2, 1′, 2, and 5′ (6.4–7.8 ppm) derived from NOB (Fig. 5b). In addition, the CH_3 group: Y (2.0 ppm), the 7-membered ring moiety: Z (1.5–1.8 ppm) derived from Sol, and the aromatic moiety derived from NOB: 2, 1′, 2′, and 5′ (6.4–7.8 ppm) (Fig. 5c). Furthermore, a cross-peak was identified between the CH_3 group derived from Sol: Y (2.0 ppm), the 7-membered ring moiety: Z (1.5–1.8 ppm), and the methoxy group, CH_3, derived from NOB: 6,8 (3.8–4.2 ppm) (Fig. 5d). EVP (ASC-DP/NOB = 1/1) was measured; however, no cross-peak was identified, suggesting no interaction occurred (data not shown). This indicated that intermolecular interactions may have occurred in Sol/ASC-DP and Sol/NOB. EVP (Sol/NOB = 8/2) was identified as dispersed over a wide range of 70–5600 nm from the particle size measurement results (Table 1); however, no precipitation was observed visually. This suggests that the interaction between Sol and NOB in NMR measurements is responsible for particle formation.

Next, interactions in the ternary system were evaluated (Fig. 6). Surprisingly, in EVP (Sol/ASC-DP/NOB=8/1/1) (Fig. 6), the Sol-derived PEG moiety X (3.6 ppm) and NOB-derived aromatic ring moieties 2, 1′, 2′, and 5′ (6.4–7.8 ppm) disappeared (Fig. 6b). In EVP (Sol/NOB = 8/2) (Fig. 5c), the cross-peaks of CH_3 group: Y (2.0 ppm), 7-membered ring moiety: Z (1.5–1.8 ppm) from Sol, and proton 2, 1′, 2′, 5′ (6.4–7.8 ppm) of aromatic ring moiety from NOB disappeared (Fig. 6c). Although a cross-peak between the 7-membered ring moiety: Z (1.5–1.8 ppm) from Sol (Sol/ASC-DP=8/2) (Fig. 4b) and the methoxy group: 6,8 (3.8 ppm) from NOB was observed, no cross-peaks were observed for EVP (Sol/ASC-DP/NOB=8/1/1) (Fig. 6d). Amazingly, CH_3 of the methoxy group from NOB: 6,8 (3.8–4.2 ppm), CH_3 group of Sol: Y (2.0 ppm), and alkyl side chain of ASC-DP: d (1.2 ppm) (Fig. 6d) could all be identified, indicating a novel interaction between the cross-peaks. Furthermore, a new cross-peak was identified between PEG structure X of Sol (3.6 ppm) and the side chains d, e (0.8–1.2 ppm) of ASC-DP (Fig. 6d). The newly identified peak was not observed for EVP (Sol/ASC-DP = 8/2) or EVP (Sol/NOB = 8/2)

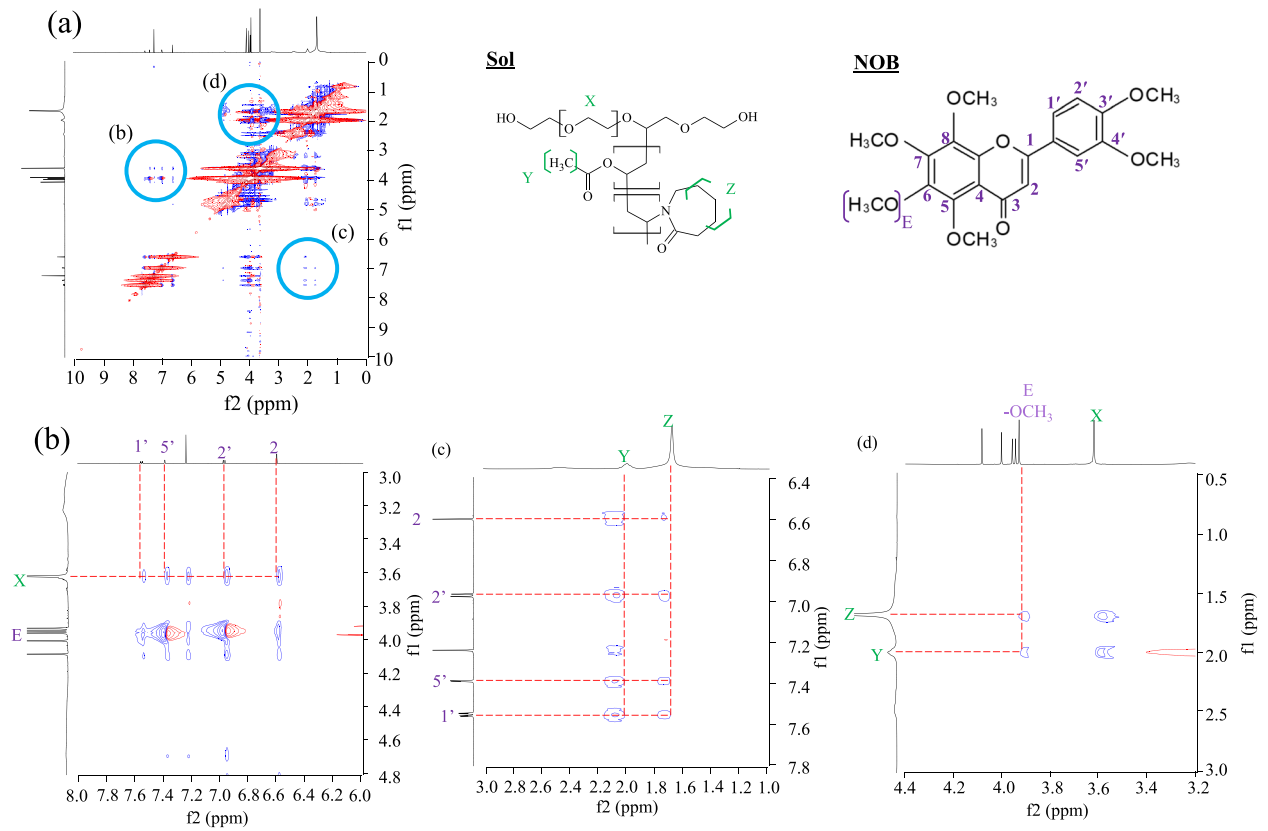

Fig. 5 ^{1}H-^{1}H ROESY NMR spectrum EVP (Sol/NOB = 8/2) in $CDCl_3$. **a** f1 is 0–10 ppm and f2 is 0–10 ppm; **b** f1 is 3.0–4.8 ppm and f2 is 6.0–8.0 ppm; **c** f1 is 6.4–7.8 ppm and f2 is 1.0–3.0 ppm; **d** f1 is 0.5–3.0 ppm and f2 is 3.0–4.8 ppm

(Figs. 4b and 5d), suggesting that it is a specific peak in the ternary system (EVP (Sol/ASC-DP/NOB = 8/1/1).

In the ternary system, the protons in the aromatic ring portion of NOB become free via the NOB methoxy group, CH_3, and the side chain of ASC-DP, the Sol CH_3 group Y, the PEG skeleton of Sol, and the side chain of ASC-DP. It was confirmed that the interactions had changed. From the above, it can be inferred that the inclusion of a component that is not a two-component system causes a change in the interaction, contributing to the formation of stable particles.

Evaluation in solid-state

Differential scanning calorimetry (DSC) measurement

From the results of NMR spectrum measurements, it is considered that the solid state before hydration affects the formation of nanoparticles. In other words, we posited that Sol/ASC-DP/NOB might have already interacted in the solid state. Therefore, to confirm the thermal behavior as an evaluation in the solid state, DSC measurements were performed (Fig. 7). For Sol, an exothermic peak derived from decomposition was confirmed at approximately 279 °C (Fig. 7a). ASC-DP has a melting point-derived endothermic peak near 58, 95, and 114 °C (Fig. 7b), NOB has a melting point-derived endothermic peak near 138 °C, and a decomposition-derived exothermic peak near 314 °C (Fig. 7c). For a single sample (Sol, ASC-DP, NOB), the endothermic peak disappeared after EVP. As a result, it was assumed that the peak did not disappear due to EVP and that EVP had no effect (data not shown). In EVP (ASC-DP/NOB = 1/1) (Fig. 7f), endothermic peaks were confirmed at approximately 71, 94, and 118 °C. In PM (Sol/ASC-DP/NOB = 8/1/1) (Fig. 7g), peaks were confirmed at 57, 95, and 128 °C, where the peaks were slightly shifted owing to the melting point depression. However, no interaction was observed in the DSC results. However, for EVP (Sol/ASC-DP=8/2) (Fig. 7d), EVP (Sol/NOB = 8/2) (Fig. 7e), and EVP (Sol/ASC-DP/NOB = 8/1/1) (Fig. 7h), the endothermic peaks derived from the melting points of ASC-DP and NOB disappeared. It was inferred that an interaction occurred between ASC-DP and NOB.

Infrared measurement

IR measurements were performed to confirm the intermolecular interactions in the solid state, suggesting the

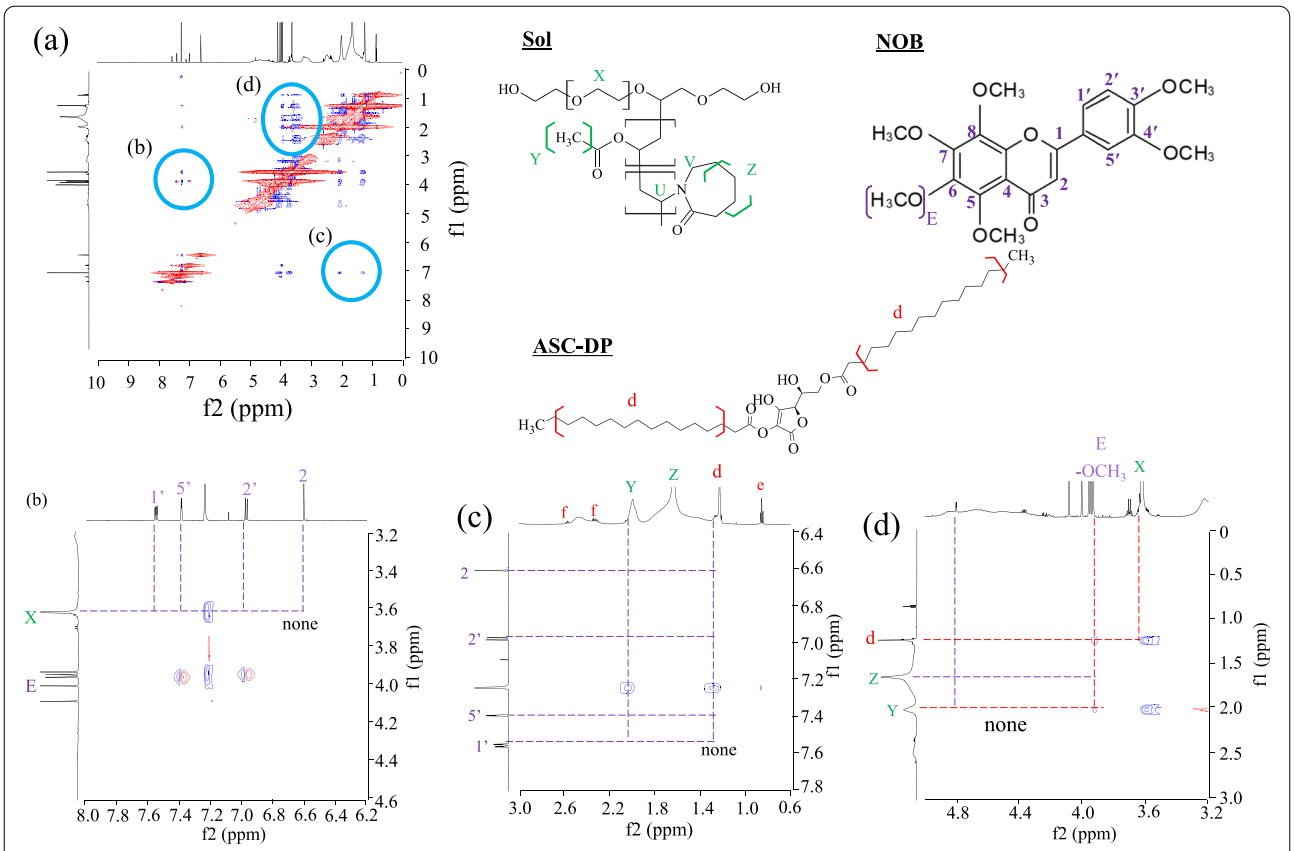

Fig. 6 ^{1}H-^{1}H ROESY NMR spectrum EVP (Sol/ASC-DP/NOB = 8/1/1) in $CDCl_3$. **a** f1 is 0–10 ppm and f2 is 0–10 ppm; **b** f1 is 3.2–4.6 ppm and f2 is 6.2–8.0 ppm; **c** f1 is 6.4–7.8 ppm and f2 is 0.6–3.0 ppm; **d** f1 is 0.5–3.0 ppm and f2 is 3.0–3.4 ppm

possibility of interaction in the solid state in the DSC. In Sol (Fig. 8a), a peak derived from C=O adjacent to the tertiary amide at 1634 cm^{-1} and a peak derived from the C=O of the ester at 1732 cm^{-1} were observed. Peaks derived from C-H stretching were confirmed at 2857 and 2922 cm^{-1}, and a peak derived from the OH group was confirmed at 3463 cm^{-1}. Because Sol has a PEG skeleton, it was inferred that the CH group of PEG contributed significantly to the peak confirmed in the CH region. In ASC-DP (Fig. 8b), a peak derived from the C=O of the ester was confirmed at 1674 cm^{-1}, and a peak derived from the C=O of the lactone ring was confirmed at 1742 cm^{-1}. The peak derived from CH stretching was confirmed at 2840–2960 cm^{-1}. A peak derived from the OH group is observed at 3453 cm^{-1}. In NOB (Fig. 8c), a peak derived from aromatic C=C was confirmed at 1519 and 1589 cm^{-1}, and a peak derived from C=O was confirmed at 1644 cm^{-1}. A peak derived from the CH group was confirmed at 2830–3010 cm^{-1}. First, in the two-component EVP (Sol/ASC-DP = 8/2) (Fig. 8d), the peak at 1732 cm^{-1} indicates the C=O of Sol ester, and the peak at 1674 cm^{-1} indicates the C=O of the ASC-DP ester, and the 1740 cm^{-1} peak from C=O on the lactone ring of ASC-DP disappeared. The disappeared peaks were shifted to the high-wavelength side of 1772 cm^{-1} and 1737 cm^{-1}. In addition, the peak of CH, which was confirmed at 2922 cm^{-1} in Sol and 2918 cm^{-1} in ASC-DP, was established by shifting to the high-wavelength side of 2925 cm^{-1}. Because Sol has a PEG skeleton, it is inferred that the peak confirmed at 2922 cm^{-1} shifted this time is derived from PEG. Furthermore, the peaks at 3463 cm^{-1} for Sol derived from the OH group and 3453 cm^{-1} for ASC-DP were broadened to the low-wavelength side. From this, it was inferred that an intermolecular interaction due to a hydrogen bond occurs between the OH group derived from the ester of Sol, the CH derived from PEG of Sol, and the OH group of ASC-DP.

In EVP (Sol/NOB = 8/2) (Fig. 8e), the peak at 1519 cm^{-1}, which is considered derived from the C=C of the aromatic of NOB, was shifted to the low-wavelength side of 1516 cm^{-1}. The 1742 cm^{-1} peak from the C=O in NOB disappeared. The peaks at 2922 cm^{-1}, derived from CH in the PEG skeleton of Sol, and 2934 cm^{-1}, derived from CH in NOB, were confirmed to shift to 2928 cm^{-1}. The peak derived from the OH group, which was confirmed at 3463 cm^{-1} in Sol, was shifted to the

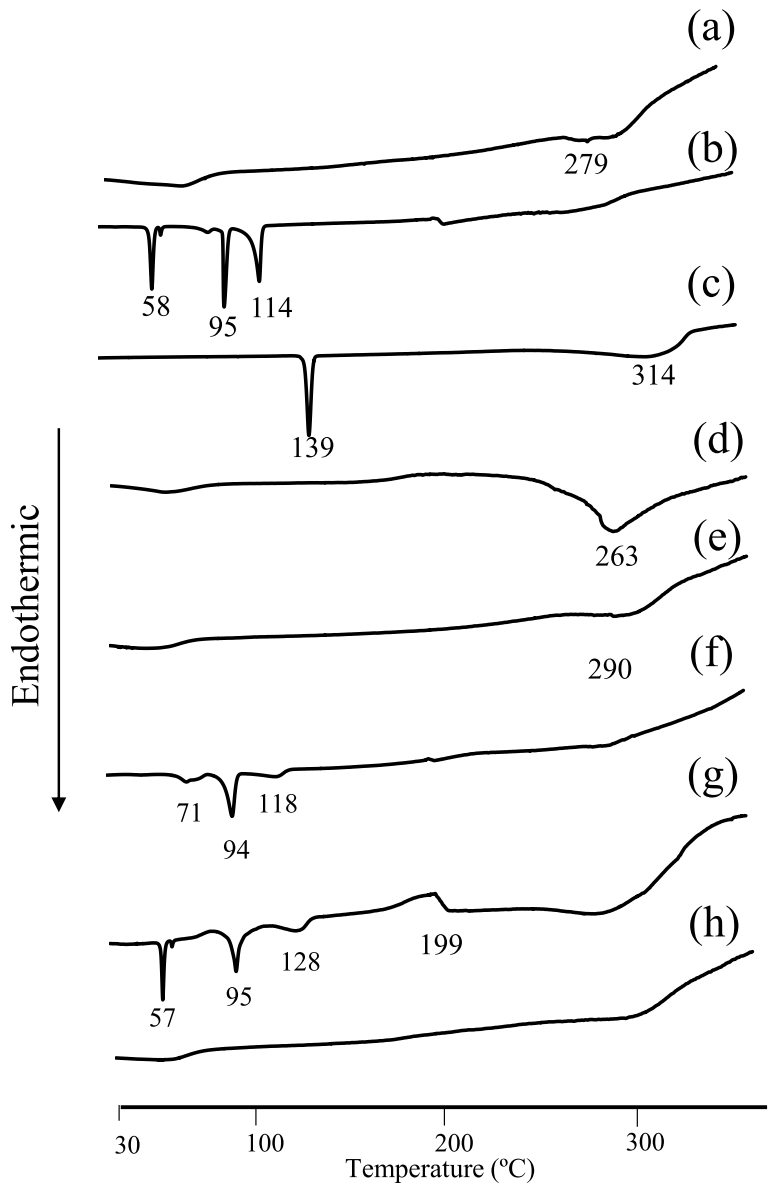

Fig. 7 DSC curves of Sol/ASC-DP/NOB systems. **a** Sol, **b** ASC-DP, **c** NOB, **d** EVP (Sol/ASC-DP = 8/2), **e** EVP (Sol/NOB = 8/2), **f** EVP (ASC-DP/NOB = 1/1), **g** PM (Sol/ASC-DP/NOB = 8/1/1), and **h** EVP (Sol/ASC-DP/NOB = 8/1/1)

low-wavelength side of 3459 cm^{-1}. From this, it can be inferred that there is a possibility that hydrogen bonds also mediate the interaction.

In EVP (ASC-DP/NOB = 1/1) (Fig. 8f), the peak at 1742 cm^{-1} attributed to the C=O of the lactone ring of ASC-DP disappeared. The disappearance of the peaks shifted to 1732–1771 cm^{-1}. In addition, the peak at 2934 cm^{-1} derived from the CH of NOB disappeared. The peak derived from the OH group, which was confirmed at 3453 cm^{-1} by ASC-DP, was shifted to the high-wavelength side of 3547 and 3471 cm^{-1}. In FT-IR, it is known that the peak derived from the OH group shifts to lower wavelengths as hydrogen bonds are formed (RajPant et al., 2010). In EVP (ASC-DP/NOB = 1/1), the peak derived from the OH group was shifted to the high-wavelength side. From this, it can be inferred that ASC-DP and NOB exist in a weak and unstable state, although an interaction due to hydrogen bonds occurs by combining them. The ternary system was then evaluated. In PM (Sol/ASC-DP/NOB = 8/1/1) (Fig. 8g), a peak derived from a single substance was confirmed, and no change was confirmed; therefore, it is inferred that no interaction occurred in PM. In EVP (Sol/ASC-DP/NOB = 8/1/1) (Fig. 8h), the peak at

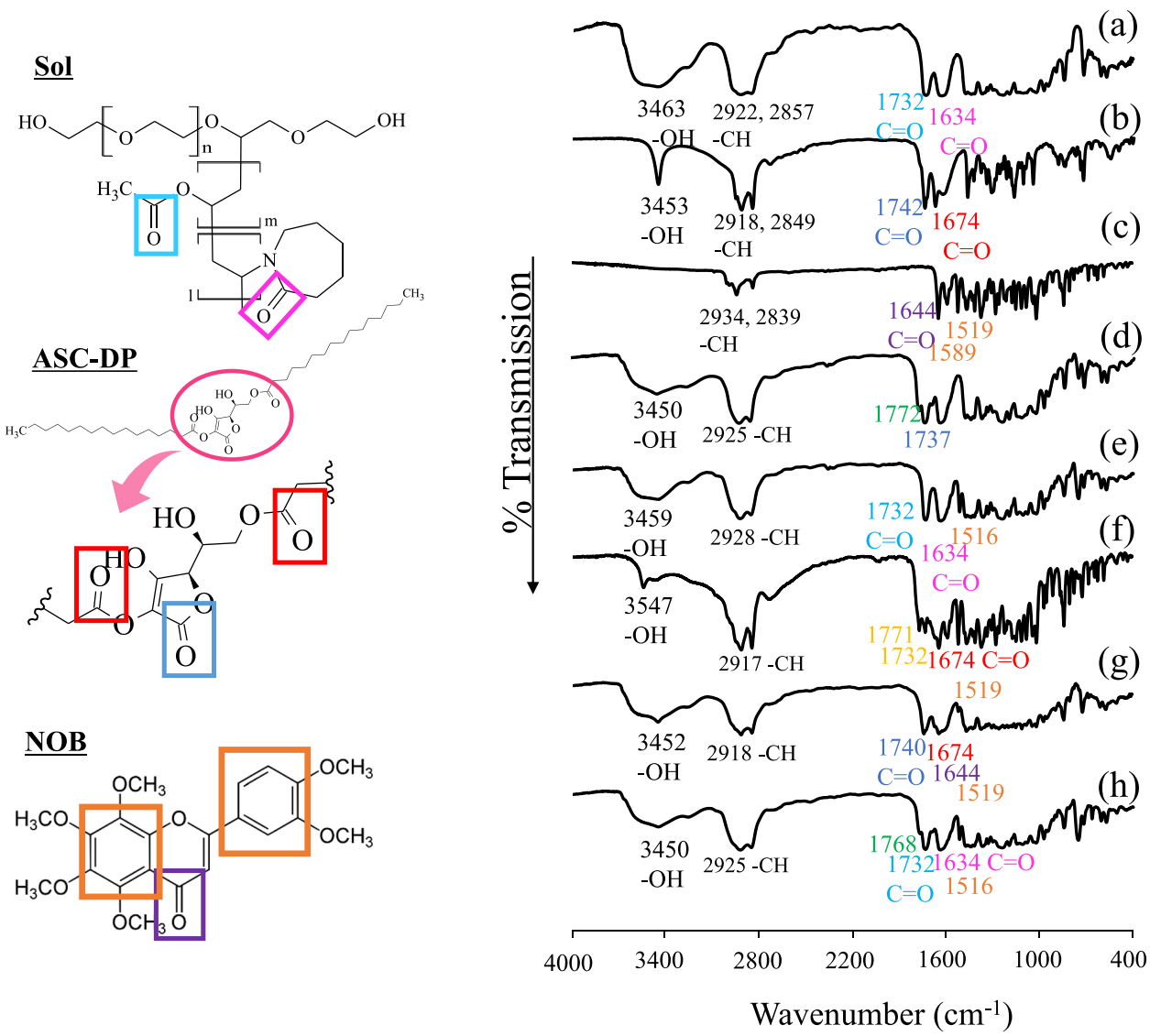

Fig. 8 FT-IR absorption spectra of Sol/ASC-DP/NOB systems. **a** Sol, **b** ASC-DP, **c** NOB, **d** EVP (Sol/ASC-DP = 8/2), **e** EVP (Sol/NOB = 8/2), **f** EVP (ASC-DP/NOB = 1/1), **g** PM (Sol/ASC-DP/NOB = 8/1/1), and **h** EVP (Sol/ASC-DP/NOB = 8/1/1)

1519 cm^{-1}, which is considered derived from the aromatic C=C of NOB, was shifted to the low-wavelength side of 1516 cm^{-1}. A peak thought to be derived from C=O of Sol was confirmed at 1732 and 1635 cm^{-1}, but the peak at 1742 cm^{-1} derived from C=O of ASC-DP disappeared and shifted to the low-wavelength side of 1770 cm^{-1}. The peak at 2922 cm^{-1}, which is thought to be the CH moiety of the Sol-derived PEG skeleton, shifted to the longer wavelength side at 2925 cm^{-1}. The peaks derived from the OH group at 3463 cm^{-1} for Sol and 3453 cm^{-1} for ASC-DP were shifted to the low-wavelength side of 3450 cm^{-1}. The new peak at 1772 cm^{-1} created by EVP (Sol/ASC-DP) was confirmed to shift to 1770 cm^{-1} at EVP (Sol/ASC-DP/NOB = 8/1/1). In addition, since the peak derived from OH was confirmed to shift to the low-wavelength side of 3450 cm^{-1}, it is inferred that the interaction was further fixed by adding NOB, and the peak shifted to the low-wavelength side.

In FT-IR, the peak derived from the OH group shifts to a lower wavelength as the hydrogen bond strength becomes stronger (RajPant et al., 2010), causing the OH peak to spread (Diaz-Visurraga et al., 2012). Therefore, in EVP (Sol/NOB = 8/2), where particle formation

was not confirmed in the solution state, the peak considered in the OH group was confirmed at 3463 cm^{-1} for Sol and 3453 cm^{-1} for ASC-DP. The peak confirmed the OH group was at 3459 cm^{-1}. In EVP (Sol/ASC-DP = 8/2) and EVP (Sol/ASC-DP/NOB = 8/1/1), where particle formation was confirmed in solution, it was confirmed that the particles were shifted toward the low-wavelength side of 3450 cm^{-1}. Broadening of the peak width was also observed, suggesting that the molecular motion was suppressed through molecular interactions. This indicates that stronger hydrogen bond-mediated interactions occur in the particles that formed even in the solid state.

Evaluation of effectiveness

DPPH radical scavenging test

The antioxidant capacity of NOB and ASC-DP was evaluated using a DPPH radical scavenging test, as NOB and ASC-DP have been reported to have the antioxidant capacity (Yia et al., 2008; Piyapong et al., 2012) (Fig. 9). The antioxidant capacity of ASC-DP alone and NOB alone showed IC_{50}: 47.8 μg/mL and 838.3 μg/mL, respectively (Fig. 9a, b). Sol alone did not exhibit any antioxidant capacity (data not shown). PM (ASC-DP/NOB = 1/1) (Fig. 9c) had an IC_{50} of 55.8 μg/mL as ASC-DP. The antioxidant capacity of EVP (Sol/ASC-DP = 8/2) (Fig. 9d) and EVP (Sol/ASC-DP/NOB = 8/1/1) (Fig. 9d) was IC_{50} 47.1 μg/mL and IC_{50} 46.7 μg/mL, respectively. Yia et al. reported that the antioxidant capacity of NOB is IC_{50} 40.97 μg/mL (Yia et al., 2008). In contrast, Danila et al. reported that NOB has a flavonoid backbone, but its antioxidant capacity is reduced owing to its methoxy group ($–OCH_3$) structure (Danila et al., 2005). In this study, the IC_{50} was 838.3 μg/mL. Therefore, it can be speculated that ASC-DP contributes to the antioxidant capacity of EVP (Sol/ASC-DP/NOB = 8/1/1) and EVP (Sol/ASC-DP = 8/2). Although EVP (Sol/ASC-DP = 8/2) and EVP (Sol/ASC-DP/NOB) formed particulates, the OH groups derived from ASC-DP did not interact with NOB or Sol, thereby maintaining the same antioxidant capacity as ASC-DP alone.

Skin permeability test and fluorescence microscope observation

First, a skin permeation test was conducted for a comparative study with intact NOB and EVP (Sol/ASC-DP/

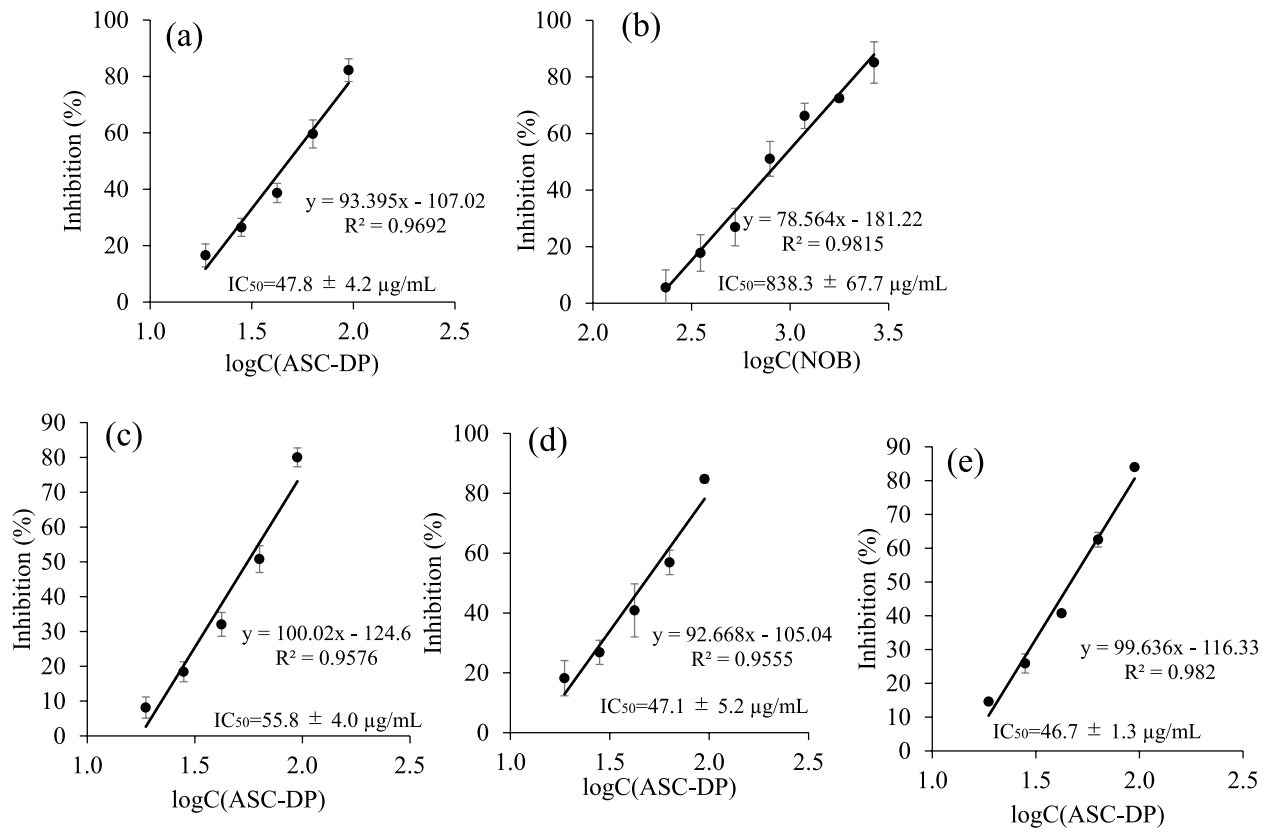

Fig. 9 DPPH radical scavenging test of Sol/ASC-DP/NOB=8/1/1 systems. **a** ASC-DP, **b** NOB, **c** ASC-DP/NOB = 1/1, **d** Sol/ASC-DP = 8/2, and **e** Sol/ASC-DP/NOB = 8/1/1. The results are expressed as the mean ± S.D. ($n = 3$)

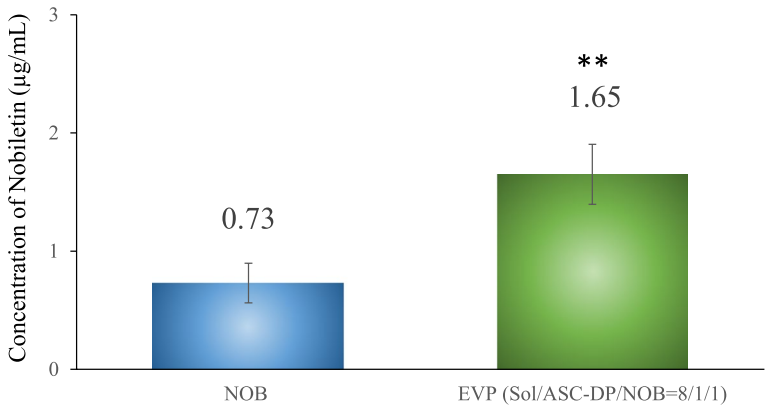

Fig. 10 Cumulative amount of transdermal NOB after 24 h. Results are expressed as means ± S.D. ($n = 3$). Tukey test. $^{**}p < 0.01$ and $^{*}p < 0.05$

NOB = 8/1/1). In pig skin permeability tests, HPLC quantification results could not confirm the permeation of NOB in the receiver compartment at 0, 1, 3, 6, and 24 h. Therefore, the effective area of porcine skin after 24 h was homogenized and measured for the residual amounts of NOB in the skin (Fig. 10). For the NOB suspension, 0.73 μg/cm^2 of NOB was retained in the skin, whereas 1.65 μg/cm^2 was held in the for EVP (Sol/ASC-DP/NOB = 8/1/1). Therefore, to confirm that NOB suspension was distributed/retained in the skin, a frozen section of YMP skin was prepared after 24 h of the skin permeation experiment and observed under a fluorescence microscope (Fig. 11). NOB fluorescence is reported as visible at approximately 480 nm (Peng et al., 2019). In the suspension of NOB alone, NOB luminescence was confined to the stratum corneum (Fig. 11a, b), whereas in EVP (Sol/ASC-DP/NOB = 8/1/1), it was observed not only in the stratum corneum but also penetrated slightly into the epidermis (Fig. 11c, d). In skin penetration and permeation of drugs, the "500 Da limit theory" must be factored into the discussion. Bos and Meinardi stated in the "500 Da Limit Theory" that drugs that can be delivered to skin tissue for local or systemic action without using transdermal absorption promoting technology are limited to hydrophobic drugs or drugs with a molecular weight of 500 or less (Bos & Meinardi, 2009). From the "500 Da limit theory," it is unlikely that the nanoparticles prepared in this study can maintain their shape and

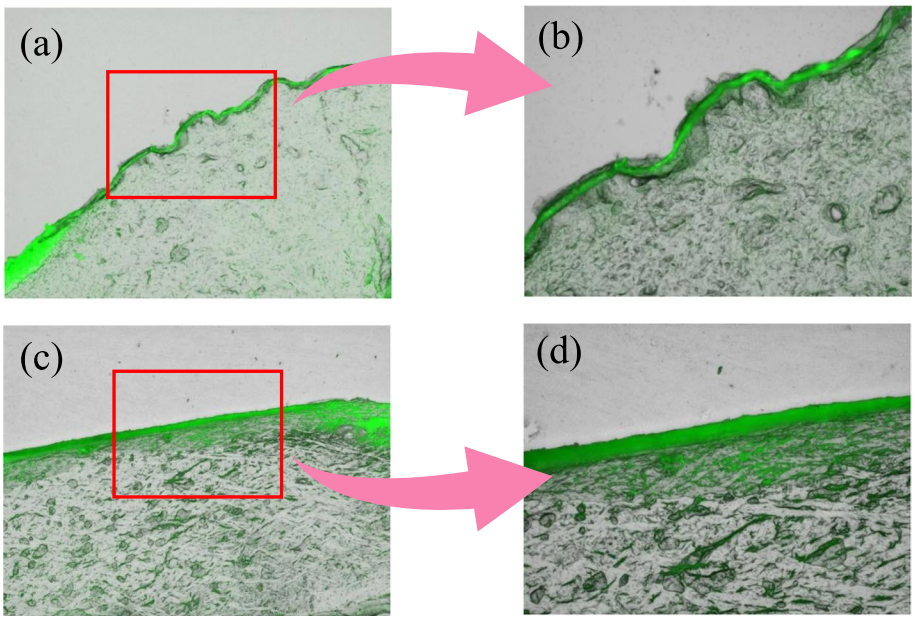

Fig. 11 Fluorescence microscope images of the epidermal side of YMP skin. **a**, **b** Intact NOB; **c**, **d** EVP (Sol/ASC-DP/NOB = 8/1/1). **a**, **c** Objective × 4; **b**, **d** objective × 4

penetrate the skin. Furthermore, it has been reported that fatty acids which have 10 to 18 carbon atoms are endogenous components of human skin and enhance the percutaneous penetration of lipophilic and hydrophilic substances (Tuntiyasawasdikul et al., 2014). Because ASC-DP contains palmitic acid with 16 carbon atoms, it may improve the transdermal permeability of NOB. Sol exhibits a surface-active effect. Surfactants have both hydrophilic and lipophilic groups and are adsorbed on the boundary surfaces of substances such as water and oil, which are inherently immiscible, to provide a bridging function. Sol and ASC-DP, being amphiphilic, forge interactions with the lipophilic and hydrophilic portions of the SC facilitating its passage. Moribe et al. (Moribe et al., 2010b) reported the preparation of microparticles by DSPE-PEG/ASC-DP and we reported the preparation of microparticles by Sol/ASCDP (Takayama et al., 2021). Notably, in this study, Sol/ASC-DP enabled the preparation of nanoparticles, further expanding the application of encapsulated NOB to the skin. Therefore, the permeability may have been improved by the surfactants, Sol and ASC-DP, with saturated fatty acids. Consequently, we speculated that NOB was observed in the skin from the EVP (Sol/ASC-DP/NOB=8/1/1) formulation.

Cell viability assay

It was confirmed that the skin permeability of NOB was improved and affirmed by the fluorescence microscope observations. Therefore, to evaluate the functionality of NOB in the skin, cell viability was measured in B16 and A375 skin-related melanoma cells, 4T1 breast cancer cells (that penetrated the skin surface), and HaCaT keratinocytes (Fig. 12). Distilled water, unaltered Sol, Sol/ASC-DP = 8/2, Sol/ASC-DP/NOB = 8/1/1, and Sol/NOB = 8/2 were added and evaluated. NOB was intact, but aggregation was observed even when dissolved in DMSO, and valid data could not be obtained; therefore, it was not used.

In A375 (Fig. 12a), a decrease of approximately 20% was confirmed at 0.2 mg/mL and 0.4 mg/mL with Sol alone. At Sol/ASC-DP = 8/2, a decrease of approximately 10% was observed at 0.1 mg/mL, but no significant difference was observed at any concentration. At Sol/ASC-DP/NOB = 8/1/1 and Sol/NOB = 8/2, both decreased in a

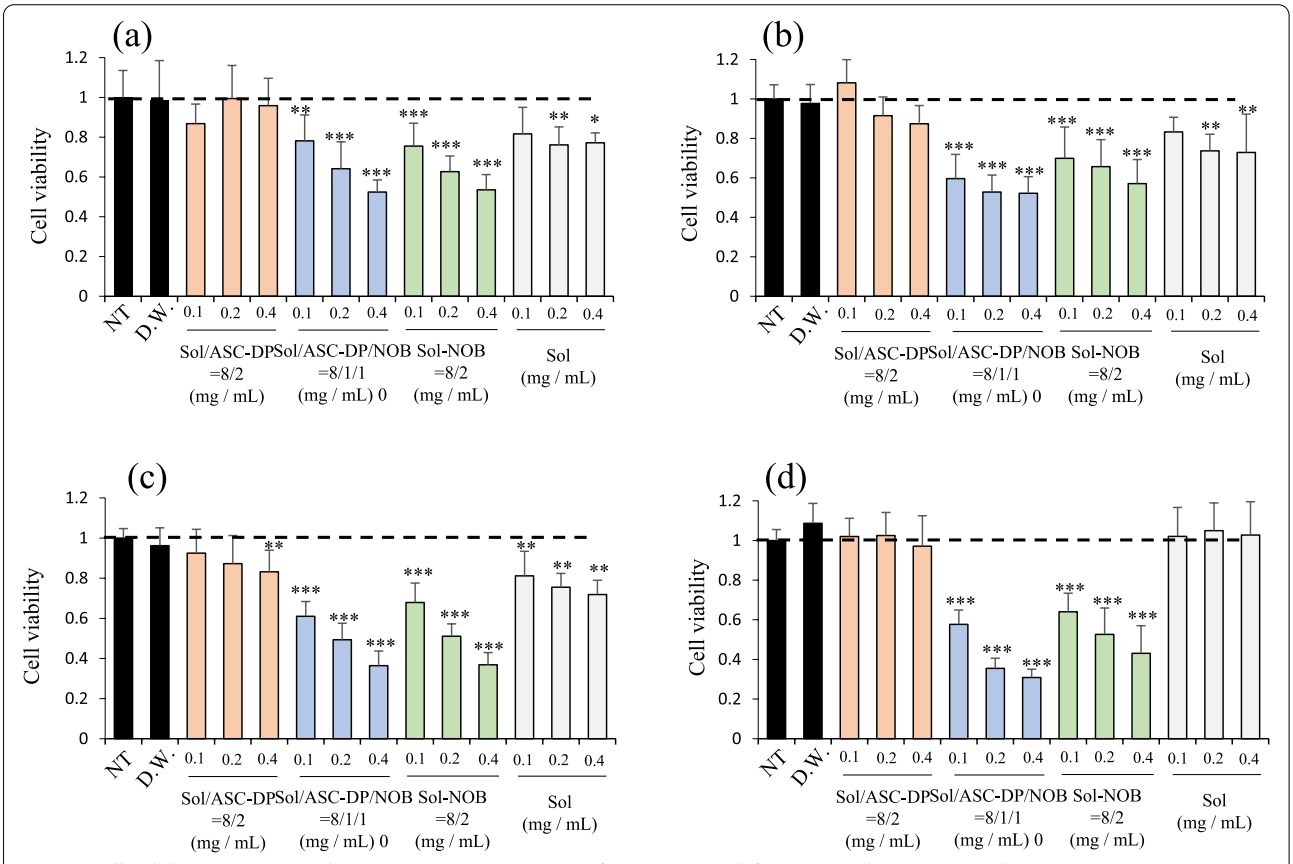

Fig. 12 Cell viability assays using Sol/ASC-DP/NOB systems. **a** A375, **b** B16, **c** 4T1, and **d** HaCaT. Results are expressed as means ± S.D. ($n = 3$). Dunnett's test, and compared with those treated with distilled water, with significant differences at ***$p < 0.001$, **$p < 0.01$, and *$p < 0.05$

concentration-dependent manner, and at 0.1 mg/mL, a significant decrease of approximately 20% was observed. Furthermore, a significant decrease of 40% or more was confirmed at 0.4 mg/mL. However, since the content of NOB in Sol/ASC-DP/NOB is half that of Sol/NOB, Sol/ASC-DP/NOB nanoparticles are suggested to have an enhanced inhibitory effect on cell proliferation. It was suggested in B16 (Fig. 12b) that unaltered Sol was confirmed to decrease 0.2 mg/mL and 0.4 mg/mL, similar to A375, by approximately 20%. At Sol/ASC-DP = 8/2, the cell number increased by approximately 10% at 0.1 mg/mL and decreased by approximately 10% at higher concentrations, but no significant difference was confirmed. At Sol/ASC-DP/NOB = 8/1/1, it decreased in a concentration-dependent manner, and a significant decrease of approximately 40% at 0.1 mg/mL and approximately 50% at 0.2–0.4 mg/mL was confirmed. A significant decrease of approximately 30% at 0.1–0.2 mg/mL and approximately 40% at 0.4 mg/mL was confirmed at Sol/NOB = 8/2. In B16 and A375, Sol/ASC-DP/NOB (8/1/1) nanoparticles were shown to enhance the inhibitory effect on cell proliferation. In 4T1 (Fig. 12c), a significant decrease of 20% or more was confirmed in unaltered Sol even at a 0.1-mg/mL concentration. At Sol/ASC-DP = 8/2, a significant decrease of 20% was confirmed at 0.4 mg/mL. A 40% decrease was confirmed at 0.1 mg/mL for both Sol/ASC-DP/NOB = 8/1/1 and Sol/NOB = 8/2. It decreased in a concentration-dependent manner, and a 60% decrease was confirmed at 0.4 mg/mL. We confirm that NOB had a stronger inhibitory effect on cell proliferation in 4T1 than A375 and B16. HaCaT (Fig. 12d) did not show a decrease in viability with Sol alone. In addition, Sol/ASC-DP = 8/2 did not show any change in cell viability as in Sol intact. However, a significant decrease of 40% at 0.1 mg/mL and 60–70% at 0.4 mg/mL was confirmed at Sol/ASC-DP/NOB = 8/1/1 and Sol/NOB = 8/2. In HaCaT cells, Sol/ASC-DP/NOB (8/1/1) nanoparticles showed cell growth inhibition at higher concentrations than the other three cell tests.

The nanoparticle formulation prepared with Sol/ASC-DP/NOB = 8/1/1 had the same inhibitory effect on cell viability, even though the NOB content was half that of Sol/NOB = 8/2 in the mixed weight ratio. With the degree of decrease in cell viability of Sol/NOB = 8/2 confirmed, this suggests that the cell proliferation inhibitory effect is enhanced when nanoparticles are prepared as Sol/ASC-DP/NOB = 8/1/1.

It has been reported that NOB has a C5 methoxy group in the flavonoid skeleton, and the hydroxylated polymethoxyflavonoid is thought to induce apoptosis in HaCaT cells, and the C3′ methoxy group also shows cell growth inhibition (Abe et al., 2018). The present NMR measurements confirmed that the protons 2, 1′, 2′, and 5′ of the aromatic portion of NOB interacted with the PEG moiety (X), methyl group (Y), and 7-membered ring portion (Z) of Sol at Sol/NOB = 8/2. Furthermore, the C6,8 methoxy group of NOB interacted with the methyl group Y and the 7-membered ring moiety Z of Sol (Fig. 5). However, in the case of Sol/ASC-DP/NOB = 8/1/1, the interaction that occurred at the aromatic moieties 2, 1′, 2′, and 5′ derived from NOB disappeared, and the interaction between the methoxy group C6,8 of NOB and the 7-membered ring moiety Z of Sol was also not observed. Furthermore, a new interaction between the methoxy group (C6,8) of NOB and the side chain (d) of ASC-DP and between the methyl group (Y) of Sol and the side chain (d) of ASC-DP were observed (Fig. 6). Consequently, Sol/ASC-DP/NOB = 8/1/1 shows the disappearance of the interaction of the aromatic moiety of NOB, which occurred at Sol/NOB = 8/2, and a difference in the interaction of the methoxy groups: C6,8. Therefore, it was speculated that the molecular mobility of the methoxy groups C3′,5 of NOB in Sol/ASC-DP/NOB = 8/1/1 was also affected, contributing to a 2-fold decrease in cell viability compared to Sol/NOB = 8/2. Based on these findings, Sol/ASC-DP/NOB = 8/1/1 is an intriguing case, suggesting the role of regulating the molecular mobility of methoxy groups C3′,5 of NOB in stable nanoparticles in the improvement of its antitumor activity.

Conclusion

For Sol/ASC-DP/NOB = 8/1/1, it was suggested that newly prepared nanoparticles using the hydration method are approximately 100 nm in size. Skin permeation tests and fluorescence microscopy confirmed its penetration and had a high deposition of NOB into the skin. In the DPPH radical scavenging test, Sol/ASC-DP/NOB had an antioxidant capacity of IC_{50} = 46.7 μg/mL as ASC-DP. Sol/ASC-DP/NOB (8/1/1) significantly suppressed A375, B16, 4T1, and HaCaT cells by 20–40% at 0.1 mg/mL concentration in cell viability measurements. The detail of Sol/ASC-DP/NOB nanoparticle formation is mainly due to the interaction between Sol, ASC-DP, an ascorbic acid derivative, and NOB, a flavonoid moiety; this information will be useful for other researchers intending to study nanoparticles containing flavonoid-based drug moieties. The formation of Sol/ASC-DP/NOB nanoparticles enhances its antioxidant capacity, anti-tumor activity, and skin deposition of NOB.

Abbreviations

NOB: Nobiletin; Sol: Soluplus®; ASC-DP: L-Ascorbyl 2, 6-dipalmitate; EVP: Solvent distillate; PM: Physical mixture; DSC: Differential scanning calorimetry; FT-IR: Fourier transform infrared spectrometer; HPLC: High-performance liquid chromatography; NMR: Nuclear magnetic resonance;

NOESY: Nuclear Overhauser effect spectroscopy; ROESY: Rotating frame nuclear Overhauser effect spectroscopy; DW: Distilled water; PEG: Polyethylene glycol; YMP: Yucatan micropig; DDS: Drug delivery system; DPPH: 2,2-Diphenyl-1-picrylhydrazyl.

Acknowledgements
The authors wish to thank Mr. Junki Tomita of the Instrument Analysis Center at Josai University for his helpful advice regarding the NMR measurements. We would like to express our deepest gratitude to Ms. Chiharu Oda for her assistance and support for this research at NPM.

Authors' contributions
Conceptualization: YI, MI; methodology: MI, SI, TT; formal analysis and investigation: MI, SI, TT, HT; writing — original draft preparation: MI, SI, YI; writing — review and editing: MI, YI, HT; funding acquisition: YI; resources: YI; supervision: YI. The author(s) read and approved the final manuscript.

Funding
This research was funded by Josai University.

Availability of data and materials
Not applicable.

Declarations

Ethics approval and consent to participate
Not applicable.

Competing interests
The authors declare no competing interests.

Author details
[1]Laboratory of Nutri-Pharmacotherapeutics Management, Faculty of Pharmacy and Pharmaceutical Sciences, Josai University, 1-1 Keyakidai, Sakado, Saitama 3500295, Japan. [2]Laboratory of Pharmaceutics and Cosmetics, Faculty of Pharmacy and Pharmaceutical Sciences, Josai University, 1-1 Keyakidai, Sakado, Saitama 3500295, Japan.

Received: 8 April 2022 Accepted: 10 October 2022
Published online: 28 November 2022

References

Abe S, Hirose S, Nishitani M, Yoshida I, Thukayama M, Tsuji A et al (2018) Citrus peel polymethoxyflavones, sudachitin and Nobiletin, induce distinct cellular responses in human keratinocyte HaCaT cells. Biosci Biotechnol Biochem. 82:2064–2071
Arce FJ, Asano N, See GL, Oshizaka T, Itakura S, Todo H et al (2020) Prediction of skin permeation and concentration of rhododendrol applied as finite dose from complex cosmetic vehicles. Int J Pharm. 578:119186
Bos JD, Meinardi MM (2009) The 500 Dalton rule for the skin penetration of chemical compounds and drugs. Exp Dermatol. 9:165–169
Danila DM, Marco G, Maurizio LG, Elisa T, Santo G, Enrico F (2005) Flavanones in citrus fruit: structure–antioxidant activity relationships. Food Res Int. 38:1161–1166
Dengning X, Hongzhen Y, Jinsong T, Jianrong Z, Quanlei Z, Chunliu Z et al (2016) Supersaturated polymeric micelles for oral cyclosporine a delivery: the role of soluplus–sodium dodecyl sulfate complex. Colloids Surf B Biointerfaces 141:301–310
Dian L, Yu E, Chen X, Wen X, Zhang Z (2014) Enhancing oral bioavailability of quercetin using novel soluplus polymeric micelles. Nanoscale Res Lett. 9:2406
Diaz-Visurraga J, Daza C, Pozo C, Becerra A, Plessing CV, Garcia A (2012) Study on antibacterial alginate-stabilized copper nanoparticles by FT-IR and 2D-IR correlation spectroscopy. Int J Nanomedicine. 7:3597–3612
Hattori T, Tagawa H, Inai M, Kan T, Kimura S, Itai S et al (2019) Transdermal delivery of nobiletin using ionic liquids. Sci Rep. 9:20191
Kameyama K, Sakai C, Kondoh S (1996) Inhibitory effect of magnesium l-ascorbyl-2-phosphate (VC-PMG) on melanogenesis in vitro and in vivo. J Am Acad Dermatol. 34:29–33
Kunimasa K, Ikekita M, Sato M, Ohta T, Yamori Y, Ikeda M et al (2010) a citrus polymethoxyflavonoid, suppresses multiple angiogenesis-related endothelial cell functions and angiogenesis in vivo. Cancer Sci. 101:2462–2469
Lai CS, Li SM, Chai CY, Lo CY, Dushenkov S, Ho CT, Pan MH, Wang YJ (2008) Carcinogenesis. 29:2415–2424
Lin N, Sato T, Takayama Y, Mimaki Y, Sashida Y, Yano M, Ito A (2003b) Biochem Pharmacol. 65:2065–2071
Lin N, Sato T, Takayama Y, Mimaki Y, Sashida Y, Yano M et al (2003a) Novel anti-inflammatory actions of nobiletin, a citrus polymethoxy flavonoid, on human synovial fibroblasts and mouse macrophages. Biochem Pharmacol. 65:2065–2071
Lin W, Yao J, Zhou JP (2009) Preparation of self-assemble nobiletin proliposomes and its pharmacokinetics in rats. Yao Xue Xue Bao. 44:192–196
Luque-Alcaraz AG, Lizardi J, Goycoolea FM, Valdez MA, Acosta AL, Iloki-Assanga SB et al (2012) Characterization and antiproliferative activity of nobiletin-loaded chitosan nanoparticles. J Nanomater. 2012:7
Matsuzaki K, Yamakuni T, Hashimoto M, Haque AM, Shido O, Mimaki Y et al (2006) Nobiletin restoring β-amyloid-impaired CREB phosphorylation rescues memory deterioration in Alzheimer's disease model rats. Neurosci Lett. 400:230–234
Meister A (1994) Glutathione-ascorbic acid antioxidant system in animals. J Biol Chem. 269:9397–9400
Mishra PR, Shaal LA, Müller RH, Keck CM (2009) Production and characterization of hesperetin nanosuspensions for dermal delivery. Int J Pharm. 371:182–189
Moribe K, Maruyama S, Inoue Y, Suzuki T, Fukami T, Tomono K, Higashi K, Tozuka Y, Yamamoto K (2010b) Ascor-byl dipalmitate/PEG-lipid nanoparticles as a novel carrier for hydrophobic. Drugs Int J Pharm. 387:236–243
Moribe K, Maruyama S, Inoue Y, Suzuki T, Fukami T, Tomono K et al (2010a) Ascorbyl dipalmitate/PEG-lipid nanoparticles as a novel carrier for hydrophobic drugs. Int J Pharm. 387:236–243
Murakami A, Nakamura Y, Ohto Y, Yano M, Koshiba T, Koshimizu K, Tokuda H, Nishino H, Ohigashi H (2000) Biofactors. 12:187–192
Nagase H, Omae N, Omori A, Nakagawasai O, Tadano T, Yokosuka A et al (2005) Nobiletin and its related flavonoids with CRE-dependent transcription-stimulating and neuritegenic activities. Biochem Biophys Res Commun. 337:1330–1336
Onoue S, Nakamura T, Uchida A, Ogawa K, Yuminoki K, Hashimoto N et al (2013) Physicochemical and biopharmaceutical characterization of amorphous solid dispersion of nobiletin, a citrus polymethoxylated flavone, with improved hepatoprotective effects. Eur J Pharm Sci. 49:453–460
Onoue S, Uchida A, Takahashi H, Seto Y, Kawabata Y, Ogawa K et al (2011) Development of high-energy amorphous solid dispersion of nanosized nobiletin, a citrus polymethoxylated flavone, with improved oral bioavailability. J Pharm Sci. 100:3793–3801
Onoue S, Yamada S, Chan HK (2014) Nanodrugs: pharmacokinetics and safety. Int J Nanomedicine. 9:1025–1037
Palma S, Manzo R, Nostro P, Allemandi D (2007) Nanostructures from alkyl vitamin C derivatives (ASCn): properties and potential platform for drug delivery. Int J Pharm. 345:26–34
Peng J, Su Y, Huang FQ, Zuo Q, Yang L, Li J et al (2019) simple and rapid fluorescent approach for flavonoids sensor based on gold nanoclusters. J Colloid Interface Sci. 539:175–183
Piyapong S, Amporn S, Panuwat S (2012) Antioxidant activities of curcumin and ascorbyl dipalmitate nanoparticles and their activities after incorporation into cellulose-based packaging films. J Agric Food Chem. 60:5388–5399
RajPant H, Bajgai MP, Yi C, Nirmala R, Nam KT, Beak W et al (2010) Effect of successive electrospinning and the strength of hydrogen bond on the morphology of electrospun nylon-6 nanofibers. Colloids Surf A Physicochem Eng Aspects. 370:87–94
Seki T, Kamiya T, Furukawa K, Azumi M, Ishizuka S, Takayama S et al (2013) Nobiletin-rich Citrus reticulata peels, a kampo medicine for Alzheimer's disease: a case series. Geriatr Gerontol Int. 13:236–238
Singh R, Lillard JW (2009) Nanoparticle-based targeted drug delivery. Exp Mol Pathol. 86:215–223

Sun T, Zhang YS, Pang B, Hyun DC, Yang M, Xia Y (2014) Engineered nanoparticles for drug delivery in cancer therapy. Angew Chem Int Ed Engl. 53:12320–12364
Takayama R, Ishizawa M, Yamada M, Inoue Y, Kanamoto I (2021) Characterization of soluplus/ASC-DP nanoparticles encapsulated with minoxidil for skin targeting. ChemEngineering. 5:44
Tanida S, Kurokawa T, Sato H, Kadota K, Tozuka Y (2016) Evaluation of the micellization mechanism of an amphipathic graft copolymer with enhanced solubility of ipriflavone. Chem Pharm Bull. 64:68–72
Tuntiyasawasdikul S, Limpongsa E, Jaipakdee N, Sripanidkulchai B (2014) Transdermal permeation of Kaempferia parviflora methoxyflavones from isopropyl myristate-based vehicles. AAPS PharmSciTech. 15:947–955
Yamaguchi K, Mitsui T, Aso Y, Sugibayashi K (2008) Structure–permeability relationship analysis of the permeation barrier properties of the stratum corneum and viable epidermis/dermis of rat skin. J Pharm Sci. 97:4391–4403
Yang H, Teng F, Wang P, Tian B, Lin X, Hu X et al (2014) Investigation of a nanosuspension stabilized by Soluplus® to improve bioavailability. Int J Pharm. 477(1-2):88–95
Yao J, Lu Y, Zhou JP (2008) Preparation of nobiletin in self-microemulsifying systems and its intestinal permeability in rats. J Pharm Pharm Sci. 11:22–29
Yia Z, Yu Y, Liang Y, Zeng B (2008) In vitro antioxidant and antimicrobial activities of the extract of Pericarpium Citri Reticulatae of a new Citrus cultivar and its main flavonoids. LWT. 41:597–603
Zeng YC, Li S, Liu C, Gong T, Sun X, Fu Y et al (2017) Soluplus micelles for improving the oral bioavailability of scopoletin and their hypouricemic effect in vivo. Acta Pharmacol Sin. 38:424–433
Zhang L, Li Y, Yu JC (2014) Chemical modification of inorganic nanostructures for targeted and controlled drug delivery in cancer treatment. J Mater Chem B. 2:452–470

Publisher's Note